Rapid liquid biopsy assessment through gene profiling from the kidney biopsy transport medium: a technical validation and a proof-of-concept pilot study

Ziyang Li[1], Marij J.P.Welters[2], Aiko P.J. de Vries[3,4], Jan A. Bruijn[1], Hans J. Baelde[1], Jesper Kers[1,4,5]

1 Department of Pathology, Leiden University Medical Center, Leiden, the Netherlands

2 Department of Medical Oncology, Oncode Institute, Leiden University Medical Center, Leiden, the Netherlands

3 Department of Internal Medicine, Division of Nephrology, Leiden University Medical Center, Leiden, The Netherlands

4 Leiden Transplant Center, Leiden University Medical Center, Leiden, The Netherlands

5 Department of Pathology, Amsterdam UMC, Amsterdam, The Netherlands

Corresponding author

Ziyang Li

Department of Pathology

Leiden University Medical Center

Albinusdreef 2, 2333 ZA, Leiden

The Netherlands

Email: z.li5@lumc.nl

Abstract

Background:

Rapid diagnosis is pivotal in kidney disease for timely and targeted treatment. Conventional microscopic and molecular assessments from biopsy tissues rely on extra sample processing (e.g., formalin-fixation, paraffin-embedding (FFPE)) or an extra biopsy core (e.g., Molecular Microscope Diagnostic System [MMDx]), making same-day diagnosis impractical. Therefore, we introduce a novel and freely accessible material, the biopsy transport medium (BTM), which can serve as a source of biomarkers with high potential and is promising for accelerating the assessment workflow.

Methods:

Biopsies were cut from tumor-free tissues obtained from nephrectomies to create BTM mimics for homogenization. We optimized the RNA extraction procedure from BTM by investigating crucial steps in the process. We measured the quantity and integrity of the RNA and different biomarkers derived from BTM through qPCR. Additionally, we performed gene signature profiling on BTM using the Banff Human Organ Transplant (B-HOT) panel in the NanoString nCounter platform as a proof-of-concept study.

Results:

The storage time (the duration a biopsy is stored in the BTM), ranging from 0.5 to 24 hours did not significantly affect RNA quality and yield. Differential gene expression analysis on allograft rejection BTM described specific profiles related to rejection. A significant correlation was observed between rejection-related transcripts and the corresponding Banff lesion scores.

Conclusion:

This study validated that the BTM can provide transcriptomic information relevant to the state of the kidney. The proof-of-concept study demonstrated that BTM has great potential for reflecting the status of the transplanted kidney. Tailored qPCR panels could allow for fast (same-day) molecular diagnosis.

Keywords: biopsy transport medium, gene profiling, fast molecular diagnosis, kidney transplantation

Introduction

Rapid diagnosis is imperative for effectively managing kidney diseases, particularly in cases of acute kidney injury (AKI), which poses a significant threat to future organ function, akin to the critical nature of myocardial infarction and cerebral stroke scenarios ('time equals tissue'). Notably, AKI, characterized by high inflammatory activity such as anti-neutrophil cytoplasmic antibody (ANCA)-associated vasculitis (AAVs) or severe acute rejection of transplanted kidneys, requires rapid diagnosis as a critical step for initiating prompt interventions like immunotherapy or plasma exchange. This can help mitigate adverse consequences and potentially reverse damage. In contrast, delays in starting tailored treatments can lead to a great loss of tissue, progression towards fibrosis and a progressive decline in organ function over time.

The current gold standard for assessing disease status involves microscopic examination after formalin fixation and tissue processing, which typically takes at least 24 hours for an initial assessment. Conventional histological analysis also faces limitations due to variability (dissension) and disagreement among specialized pathologists, which can further delay a final diagnosis. While emerging molecular technologies offer potential advancements, such as the Molecular Microscope Diagnostic System [MMDx] and the NanoString Banff Human Organ Transplant (B-HOT) targeted gene profiling system, these technologies face significant challenges. MMDx requires additional biopsy cores, and B-HOT profiling necessitates further sample processing of formalin-fixation, paraffin-embedding (FFPE) material, limiting their accessibility in clinical practice[1, 2]. In most settings, molecular biopsy profiling will be performed only after histological assessment is equivocal (e.g., rejection vs. no rejection).

In response to these limitations, we are currently exploring alternative methods to overcome these barriers by investigating a novel and freely accessible liquid biopsy. At the LUMC, kidney biopsies are performed by interventional radiologists and promptly transported to the pathology ward floating in 0.9% buffered NaCl (no gause), with a total transport time of approximately 30 minutes. The pathology department processes the biopsy, and the biopsy transport medium (BTM) is typically discarded. However, the BTM may contain a diverse array of tissue-derived molecules, vesicles, and

intact (live) cells, providing a broad range of biological information for diagnostic purposes and potentially functional tests.

In this study, our objectives were: 1) to validate the technical feasibility of utilizing the BTM as a source of molecular information, and 2) to present a proof-of-concept study demonstrating that gene signature profiling from the BTM could provide actionable information to classify rejection (subtypes) versus non-rejection in the commonly encountered clinical scenario of delayed graft function.

Materials and Methods

Samples and processing

The kidney biopsy procedure at LUMC typically involves two routine needle passes, utilizing a 16G needle. Two biopsies are then acquired, each measuring 15-20 mm in length and approximately 1 mm in diameter. To standardize the condition of the BTM, we mimicked the renal biopsy procedure by harvesting tumor-free tissues from a tumor nephrectomy. These tissues were cut into slices of 1.5x1.5x20 mm, close to real kidney biopsies, and processed accordingly. Pairs of tissue pieces were then placed in 15 ml phosphate-buffered saline (PBS). In addition, two larger pieces of the adjacent tissue from the same nephrectomy were processed either as FFPE or fresh-frozen samples which were stored at -80 □. Before centrifuging BTM, biopsies were removed, and the resulting sediments were lysed with 500 µl TRIzol™ Reagent (Ambion, Foster City, CA, USA) or 350 µl buffered RLT (included in RNeasy Micro Kit, QIAGEN, Hilden, Germany) + 3.5 µl 2-Mercaptoethanol (Merck Schuchardt OHG, Hohenbrunn, Germany) and homogenized. After RNA isolation, the RNA yield was estimated by measuring its concentration. Concurrently, we prospectively collected and processed BTM derived from real renal biopsies in the pathology ward for later selection. All the materials were obtained, completely anonymized (i.e. no pseudonymization code was put in place and no clinical data were retrieved from the electronic health records), and handled according to institutional guidelines, Good Research Practice, in accordance with Dutch national ethics guidelines according to (the Code of Conduct for the Proper Secondary Use of Human Tissue).

Analyzing RNA extraction methods: a procedural comparison of BTM mimics

To examine the effect of storage time (the duration a biopsy is floating in the BTM during transport/storage) on the quantity and integrity of RNA molecules, we set up five groups with varying storage times, 0.5 hours, 1 hour, 2 hours, 4 hours, and 24 hours. During the initial 0.5 hours, samples were kept at room temperature in BTM and subsequently transferred to a 4 °C refrigerator after the initial 0.5 hours mimicking clinical practice. Biopsies were removed from the BTM at different time intervals, and the resulting BTM underwent centrifugation. To examine the effect of centrifuge speed on the RNA yield, we set up two groups with centrifuge speeds of 1500g and 3000g for 5 minutes. Plus, due to the relatively low RNA yield in the BTM, we employed both the TRIzol method and the RNeasy Micro Kit to compare the efficiency of these two RNA isolation methods. Meanwhile, to further optimize the aforementioned methods, we set up two groups: 1) RNeasy without DNase treatment versus RNeasy with DNase treatment (DNase treatment is an optional procedure in the manufacturer's instructions); 2) TRIzol method versus TRIzol method plus RNeasy clean-up (QIAGEN, Hilden, Germany).

RNA quantity and integrity assay

RNA concentration was measured with the Qubit RNA HS Assay Kit on the Qubit 2.0 Fluorometer (Thermo Fisher Scientific, Waltham, MA, USA) according to the manufacturer's instructions. RNA integrity was assayed using the Agilent 2100 Bioanalyzer System(Agilent Technologies, Santa Clara, CA, USA).

Analyzing gene expression in BTM mimics by qPCR

The RNA was synthesized into cDNA for qPCR analysis, utilizing IQTMSYBR Green Supermix (Bio-Rad, Hercules, CA, USA) in conjunction with the Bio-Rad CFX96 Touch Real-Time PCR Detection System and the Bio-Rad CFX Maestro 2.2 (5.2.008.0222) software. The RNA quantity was indirectly estimated through the relative quantity of the housekeeping gene hypoxanthine phosphoribosyl transferase (*HPRT*), using the formula: Relative Quantity = 2^((Cq(control) - Cq(sample))). To elucidate the distribution of cells released into the BTM, qPCR was employed to

detect the expression of several cell-specific genes: *CD20*, *CD3E*, *CD56*, *CD68*, *CD138*, *PECAM1*, *NPHS1*, and *LRP2*. These genes serve as biomarkers for B cells, T cells, NK cells, macrophages, plasma cells, endothelial cells, podocytes, and tubular epithelial cells, respectively (Table 1). The expression levels of the target genes within a sample normalized by *HPRT* and calculated by the ΔΔCt model and were expressed as 2^ΔΔCt.

Table 1 Primers

Transcript	Forward primer	Reverse primer
HPRT	TGACACTGCAAACAATGCA	GGTCCTTTTCACCAGCAAGCT
CD20	GGGGCTGTCCAGATTATGAA	CCAGGAGTGATCCGGAAATA
CD3E	CCGCCATCTTAGTAAAGTAACAG	AATACCACCCATTTCTTCATTACC
CD56	AGGCTGAGTACATCTGCATTGC	GAGTGACCTGCTCCTCTAATTCC
CD68	TTCCCCTATGGACACCTCAG	TTGTACTCCACCGCCATGTA
CD138	GCTCTGGCTCTGGCTGTG	CTGCGTGTCCTTCCAAGTG
PECAM1	AGACGTGCAGTACACGGAAG	TTTCCACGGCATCAGGGAC
NPHS1	AGGACCGAGTCAGGAACGAAT	CTGTGAAACCTCGGGAATAAGACA
LRP2	GCTGATAAAACGAGACGCACAGTA	AGGACGGAACCAATCAGTGAAG

NanoString B-HOT gene expression analysis in mimicked and real BTM

The Banff Human Organ Transplant (B-HOT)[3] code set, comprising 770 genes, was employed to analyze gene expression in RNA isolated from BTM mimics, along with corresponding frozen and FFPE samples, as well as real BTM. The analysis was conducted using the NanoString nCounter MAX Analysis system ((Nanostring Technologies, Seattle, WA, USA). Hybridization of RNA samples with the probes occurred at 65°C for 17 hours, followed by loading onto the nCounter Prep Station in accordance with the manufacturer’s instructions. Following data collection with the nCounter MAX Digital Analyzer, a preliminary analysis was conducted using the nSolver 4.0 Analysis Software System, including quality control (QC) based on Imaging QC, Binding Density QC, Positive Control QC, and Limit of Detection QC. Samples that passed QC were subjected to a two-step data transformation process (positive control normalization and housekeeping gene normalization), and normalized counts were exported for subsequent differential gene expression (DGE) analysis.

Statistical analysis

IBM SPSS Statistics 29.0.0.0 software was used for the comparative and agreement analysis. The differences in RNA yield across five storage time groups (RNA yield [ng] = RNA concentration [ng/μl] × volume [μl]) were examined through one-way ANOVA. The RNA integrity (RIN) values of RNA isolated by different procedures were compared with the Independent-Samples T-test. To explore the interactions between storage times, centrifuge speed, and RNA isolation methods and their effects on RNA yield, HPRT relative quantity qPCR data were analyzed using three-way ANOVA. Logarithmic transformation was applied to ensure normal distribution for the analyses. The inter-assay coefficient of variance (ICV) was calculated to assess variability between different assays. Column bar graphs, based on means with standard deviations (SD) were generated by GraphPad Prism 9.3.1(471). The agreement of B-HOT gene expression between BTM versus FFPE, and BTM versus frozen samples was assessed by computing intraclass correlations (ICC), which were calculated from linear mixed effects statistical models with random effects of kidneys and genes. The appropriateness of the models was examined visually by histograms of the residuals from each of the two models. The corresponding visualization was displayed via Bland-Altman plots. The DGE analysis and the corresponding visualization were implemented by RStudio-4.2.3 in Windows 10. DGE analysis utilized the "DESeq2-1.38.3" package (downloaded from https://bioconductor.org/packages/release/bioc/html)". The heatmaps were generated with the 'pheatmap-1.0.12' package". The volcano plots were generated with the 'tidyverse-2.0.0' and 'ggrepel-0.9.4' packages. The Bland-Altman Plots were generated with the ggplot2-3.4.4' packages.

Results

RNA yield of BTM mimics

Tumor-free tissues were collected from 10 nephrectomies, and a total of 120 samples were made into BTM mimics (12 identical samples were made from 1 kidney) (Figure 1). The average RNA yield was

702.09±612.91 ng per sample, and the RNA yield among the five storage time points did not significantly differ (P=0.99) (Figure 2a).

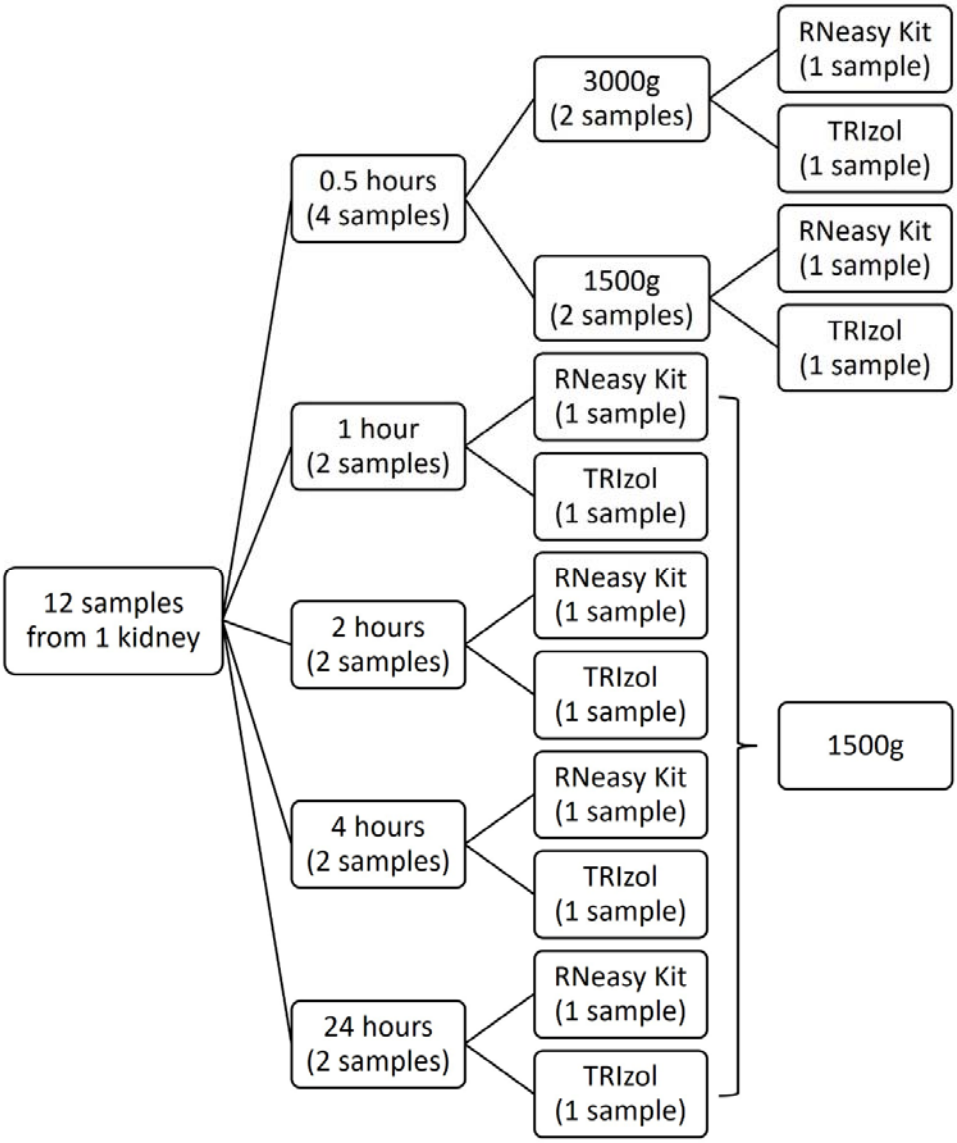

Figure 1. Workflow of procedure of the comparisons. Three factors that potentially affect the RNA yield were tested: storage times, centrifuge speed, and RNA isolation methods. Each sample consists of 2 biopsies with 15 ml of PBS. There are 12 samples in total, 2 samples were assigned to each storage time point group, except for the 0.5 hours group, to which 4 samples were assigned. Then, the two samples of each storage time point group, except for the 0.5 hours group, were divided into 2 groups (one that was isolated by the TRIzol method and the other one by RNeasy Kit) after centrifuging at the speed of 1500g. The four samples of the 0.5 hours group were divided into 2 groups, one was centrifuged at the speed of 3000g, and another at the speed of 1500g. Following that, 2 samples in each speed group were equally divided into 2 RNA isolation method groups.

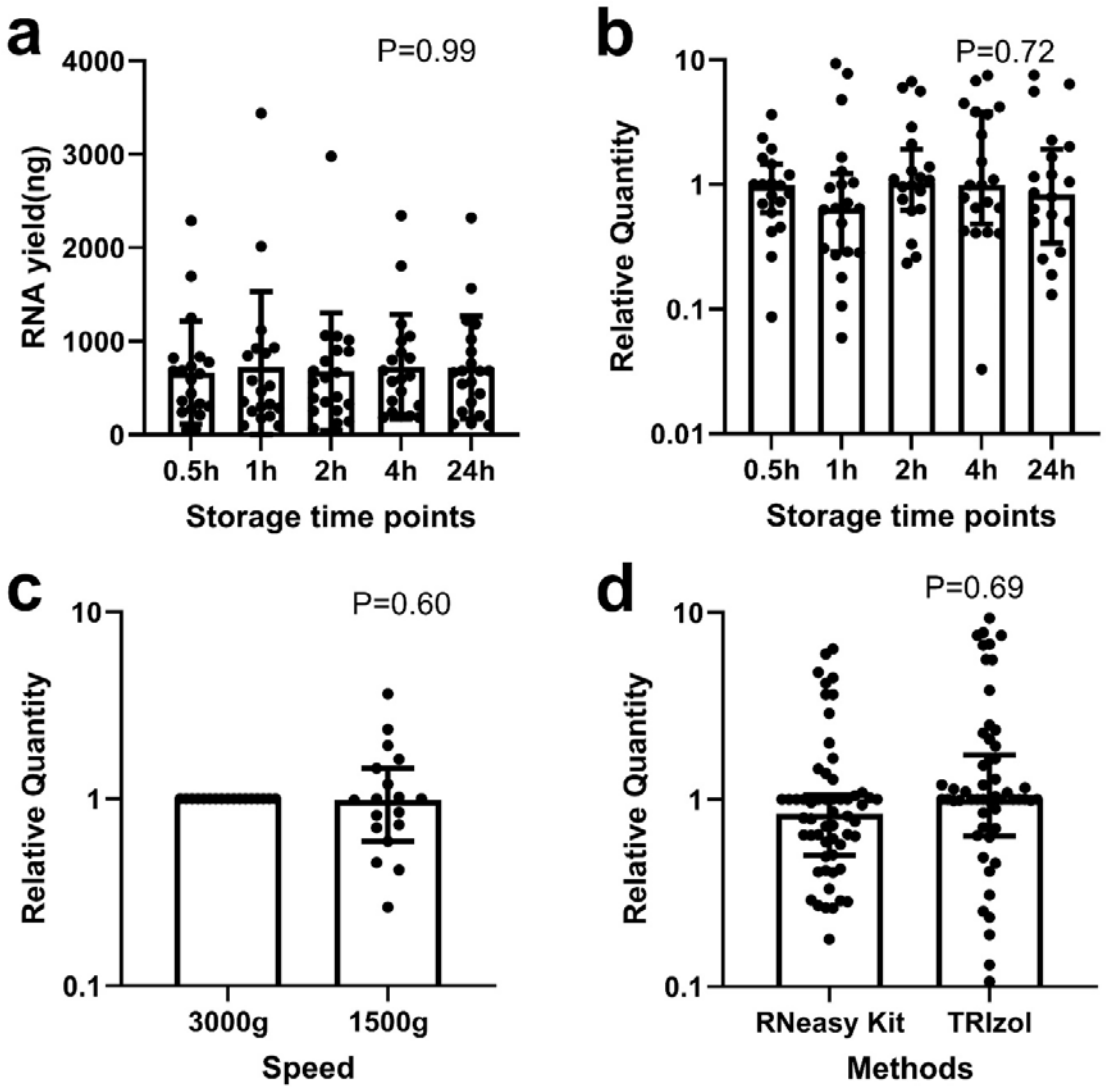

Figure 2 The average RNA yield and results of procedural comparison. (a) The average RNA yield (ng per sample) at different storage time points and the differences were tested by one-way ANOVA. (b,c, and d) The median with interquartile range value of three procedural comparison groups. The y-axis represents the relative quantity of HPRT expression normalized on each kidney by calculating the ratio between each storage time point and the corresponding 3000g value. Bar height represents the median values and error bars represent the interquartile range. The differences were tested by three-way ANOVA.

RNA integrity assessment on BTM mimics

First, RNA integrity was assessed of RNA isolated from the BTM using TRIzol or the RNeasy Kit. A total of 24 BTM mimic samples were obtained from the same nephrectomy and were evenly divided into four groups, each using a different isolation protocol (TRIzol alone, TRIzol plus RNeasy clean-up, RNeasy without DNase treatment, and RNeasy with DNase treatment). Both methods, TRIzol alone(Supplementary Figure 1a) and TRIzol + RNeasy clean-up (Supplementary Figure 1b) exhibited

positive indicators of intact RNA, with distinct 18S and 28S ribosomal RNA bands. However, the TRIzol plus RNeasy clean-up group displayed a higher RIN value and more reproducible values. Comparing RNeasy without (Supplementary Figure 2a) and with DNase treatment (Supplementary Figure 2b), the former showed dark backgrounds and broad peaks between the 18S and 28S bands, suggesting DNA contamination, which was absent in the latter. The mean RIN values for RNeasy without DNase and RNeasy with DNase were 5.18±1.34 and 7.55±0.54, respectively (P=0.006).

Procedural Effects on RNA Quantified by qPCR

HPRT housekeeping gene expression was detected in all samples, with a mean quantification cycle (Cq) of 27.05 ± 2.12. The median with interquartile range of normalized relative quantity of HPRT across different storage times was consistent: 0.99 (0.59, 1.46) for 0.5h, 0.65 (0.29, 1.22) for 1h, 1.04 (0.62, 1.92) for 2h, 0.99 (0.48, 3.79) for 4h, and 0.83 (0.34, 1.92) for 24h (P = 0.72, Figure 2b). For centrifuge speed, the median with interquartile range of relative quantity of HPRT was comparable: 1.00 for 3000g vs. 0.99 (0.59, 1.46) for 1500g (P = 0.60, Figure 2c). Regarding RNA isolation methods, the median with interquartile range of relative quantity was 0.84 (0.50, 1.06) for the RNeasy Kit vs. 1.00 (0.64, 1.73) for the TRIzol method (P = 0.69, Figure 2d). These results suggest that storage times, centrifuge speed, and RNA isolation methods do not significantly affect RNA yield as estimated by relative HPRT expression.

Furthermore, to assess qPCR reproducibility on the BTM, two randomly selected samples were measured twelve times. The amplification and melt peak curves showed high similarity (Supplementary Figure 3). The calculated ICVs for the two samples were 0.24% and 0.77%, respectively, indicating excellent consistency and technical repeatability of qPCR measurements.

Cell-specific marker expression measurement on BTM mimics by qPCR

Our selected biomarkers encompass immune cells (*CD3E*, *CD20*, *CD56*, *CD68*, and *CD138*) and parenchymal cells (*PECAM1*, *NPHS1*, and *LRP2*). While all markers are detectable in the BTM, there is a distinct cell distribution compared to corresponding frozen biopsy tissues (Figure 3). Normalized expression levels of immune cell-related biomarkers, particularly *CD3E* (5.21-fold increase, P < 0.001)

and *CD68* (5.62-fold increase, P = 0.012), are significantly higher in BTM compared to frozen tissue. Conversely, *NPHS1* expression (podocytes) is significantly lower in BTM compared to frozen tissues (0.18-fold decrease, P < 0.001). The expression of *PECAM1* (endothelial cells) and *LRP2* (proximal tubular epithelial cells) did not show significant differences between BTM and frozen tissue (P = 0.393 and P = 0.446, respectively).

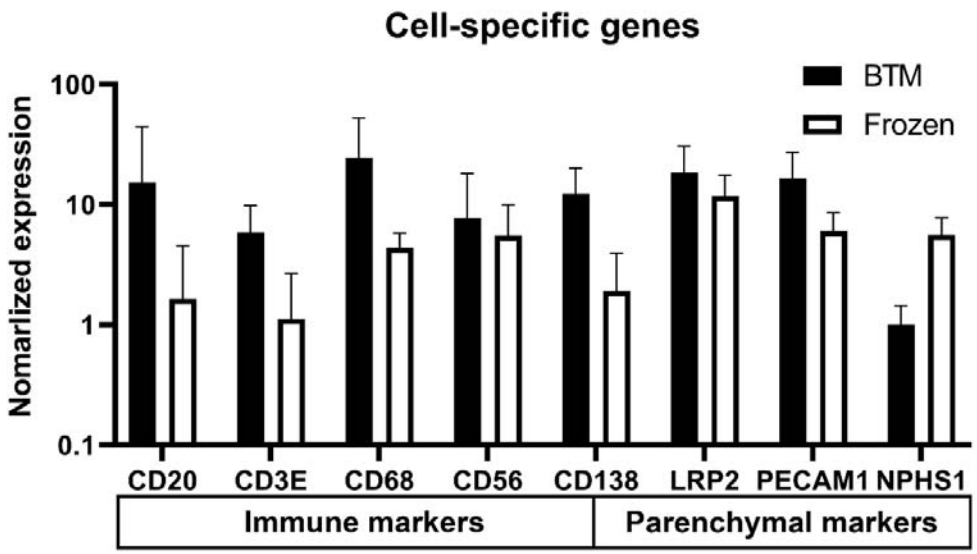

Figure 3. Cell distribution in BTM mimics compared to the corresponding biopsies. We preferentially detect immune markers relative to parenchymal markers (e.g., nephrin for podocytes) using BTM compared to RNA from the corresponding frozen biopsy material. *CD138* (encoding Syndecan-1) is expressed in both immune cells (plasma cells) and tubular epithelial cells.

NanoString B-HOT gene panel analysis on BTM mimics samples and corresponding FFPE and frozen biopsy materials

Initially, 12 samples, including BTM, FFPE, and frozen tissues from three nephrectomies, were used for B-HOT gene profiling (770 genes). From one control kidney, BTM obtained at different storage time points was assessed (Table 2). All QC measurements fell within ideal range, ensuring RNA extracted from BTM was suitable for gene expression analysis on the NanoString nCounter platform. Gene expression analysis using the B-HOT panel (770 genes) showed a strong correlation among the five different storage time points (Supplementary Figure 4), suggesting negligible effects of storage times within 24 hours on gene expression analysis. Subsequently, two groups were established based

on sample types (BTM vs FFPE, and BTM vs frozen tissues). Bland-Altman plots displayed the difference in B-HOT panel gene expression between the samples from the same nephrectomy but of different types of handling (Figure 4). We expect 95% of the ratio (BTM/frozen) will fall within the range $10^{\wedge -0.84}$ to $10\wedge^{0.59}$ (0.14-3.89), and 95% of the ratio (BTM/FFPE) will fall within the range $10^{\wedge -0.95}$ to $10^{\wedge 1.03}$ (0.11-10.72). The ICC between BTM and frozen is 0.76, and between BTM and FFPE is 0.62 (Table 3). To elucidate gene expression variations between BTM and FFPE, DGE analysis was performed between BTM and FFPE. A total of 98 genes were found to be higher expressed in BTM, while 92 genes exhibited higher expression in FFPE (adjusted p-value < 0.05 and |log2FC| > 1) (Figure 5a). To deepen understanding, the genes that showed greater differences between BTM and FFPE (adjusted p-value < 0.05 and |log2FC| > 2.5) were selected, totaling 68 DGEs. We investigated the allocation of these genes into the identified single-cell type clusters within kidney tissues through https://www.proteinatlas.org/[4]. The BTM group displayed a higher proportion of immune cell gene expression compared to FFPE (74% vs. 15%), while the FFPE group exhibited a higher proportion of genes expressed in parenchymal cells compared to BTM (27% vs. 9%) (Figure 5b). These results corroborate previous qPCR results, indicating enrichment of immune cell transcripts in the BTM compared to the corresponding biopsy tissue.

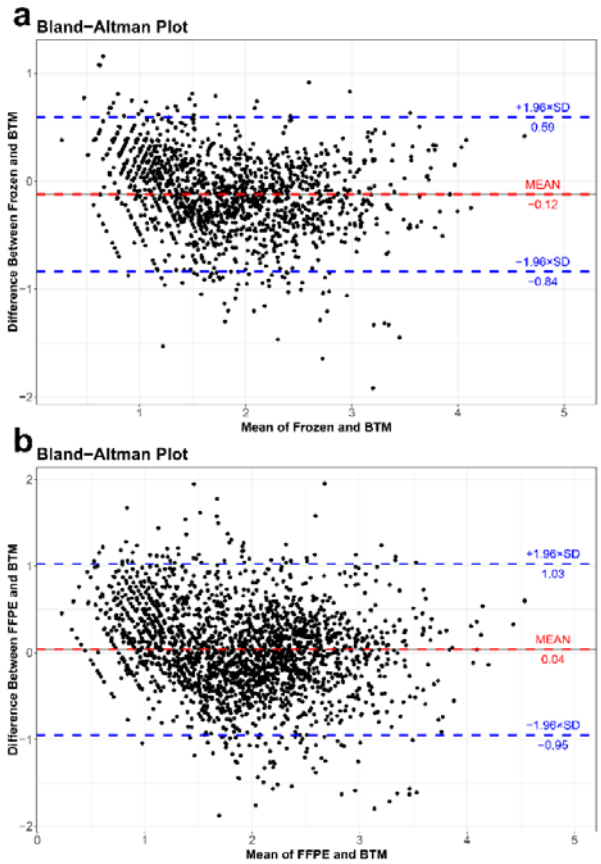

Figure 4. Bland-Altman plots of the difference in B-HOT panel expression between the samples from the same nephrectomy but different types. Each dot represents the individual difference between the two types of samples. The blue lines are the upper and lower limits of agreement, representing the range within which 95% of the differences between the two types of samples fall. The red lines represent the mean difference, indicating any systematic bias. The analysis is based on a log10 scale. When back-transformed to the original scale, the results would be interpreted as follows: a) between BTM and Frozen, we expect 95% of the ratio (BTM/Frozen) will fall within the range of $10^{-0.84}$ to $10^{0.59}$ (0.14-3.89); b) between BTM and FFPE, we expect 95% of the ratio (BTM/FFPE) will fall within the range of $10^{-0.95}$ to $10^{1.03}$ (0.11-10.72).

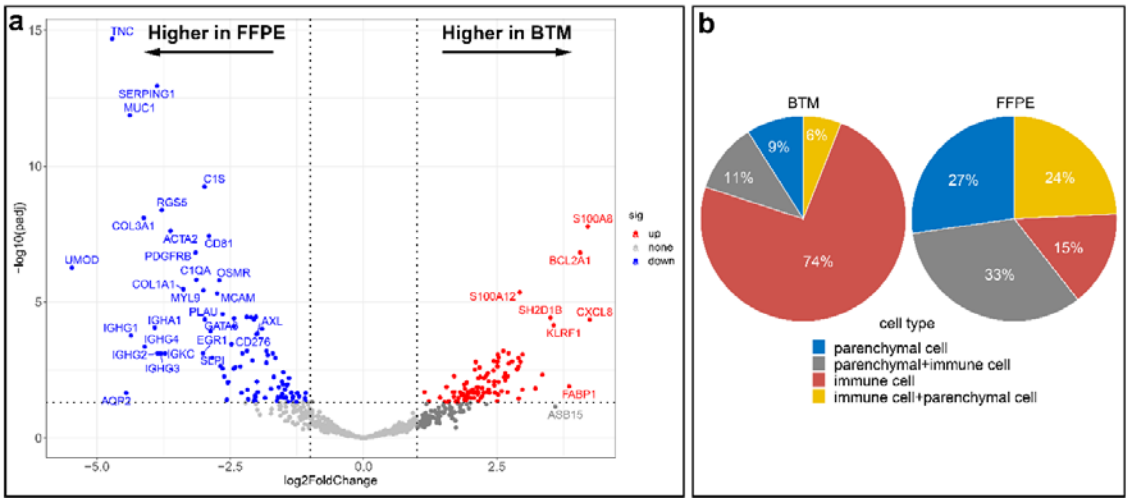

Figure 5. The difference in gene distribution between BTM mimics and the corresponding FFPE. (**a**) The volcano plot depicts B-HOT panel gene expression in BTM (kidney 1 (mean of five storage time points), kidney 2, and kidney 3) and FFPE (kidney 1, kidney 2, and kidney 3). Each colored dot represents a gene. The fold change (FC) is the ratio of mRNA count in BTM to FFPE. The X-axis represents the log2FC values. The 2 dotted vertical lines on either side of 0 on the X-axis represent |log2FC| = 1. The Y-axis represents the -log10 adjusted P value. The horizontal dotted line on the Y-axis represents adjusted p-value=0.05. The blue and red dots are genes that are |log2FC| > 1 and have an adjusted p-value < 0.05. Thus, red dots represent statistically significant DEGs that are increased in BTM compared with FFPE, and the blue dots represent the relative increase in FFPE. Of the 770 genes, 98 were increased and 92 were reduced in BTM. (**b**) Pie charts show the proportion of different cell types, that are enriched by 68 overexpressed DEGs(|log2FC| > 2.5). Parenchymal cell + immune cell means mRNA expressed in both cell types, but parenchymal cells account for the majority. Immune cell + parenchymal cell means mRNA expressed in both cell types, but immune cells account for the majority.

Table 2 Characteristics of the samples selected for the comparison of different time points of BTM versus the corresponding FFPE and frozen material.

Sample	Kidney Number	Sample type	RNA concentration (ng/μl)	RIN	Input (ng)	Imaging QC	Binding Density QC	Positive Control QC	Limit of Detection QC	FOV Count	FOV Counted
1	1	BTM-0.5h	33.8	8.2	100	0.98	0.13	0.97	9.57	490	480
2	1	BTM-1h	93.4	6.8	100	1	0.15	0.97	10.4	490	488
3	1	BTM-2h	51.2	7	100	1	0.15	0.98	12.79	490	488
4	1	BTM-4h	12.3	7.7	86.1	0.99	0.11	0.95	9.16	490	487
5	1	BTM-24h	26	7.9	100	1	0.15	0.98	8	490	489
6	1	FFPE	97.4	2.6	300	0.99	0.74	0.98	18.71	490	484
7	1	Frozen	200	6.5	100	0.98	0.22	0.97	9.5	490	481
8	2	BTM	25	7.7	50	0.98	0.13	0.98	9.94	490	481
9	2	FFPE	79.2	2.3	300	0.99	0.4	0.98	18.46	490	486
10	2	Frozen	118	6.7	100	0.99	0.22	0.98	11.13	490	485
11	3	BTM	8.48	5.6	59.36	1	0.13	0.98	11.03	490	490
12	3	FFPE	95.2	2.1	300	0.98	0.44	0.98	17.59	490	480

* The nCounter Nanostring platform was conducted for gene profiling using the B-HOT panel. Quality control was done according to the guidelines of Nanostring. Abbreviations: FOV, Field of View, RIN, RNA integrity number, QC, quality control.

Table 3 Estimates of Covariance Parameters via Intraclass Correlation Analysis

Comparison Group	Parameter	ICC	Estimate	Std. Error	Wald Z	p-value	95% Confidence Interval	
							Lower Bound	Upper Bound
BTM vs Frozen	Residual		111.83	2.87	38.92	< 0.001	106.34	117.60
	Kidney Variance	**0.76**	0.45	0.56	0.79	0.431	0.04	5.35
	Genes Variance		361.40	19.73	18.31	< 0.001	324.72	402.23
BTM vs FFPE	Residual		162.77	3.74	43.52	< 0.001	155.61	170.27
	Kidney Variance	**0.62**	0.45	55.80	0.81	0.418	0.40	5.08
	Genes Variance		266.91	15.13	17.65	< 0.001	238.85	298.27

* To speed up computations, we first transformed the data by dividing every RNA expression by 100. This does not affect the ratio. Abbreviations: ICC, intraclass correlation coefficient; Std. Error, standard error.

Table 4 Characteristics of the samples selected for the proof of principle run of clinical samples

Sample	Sample type	RNA concentration (ng/µl)	RIN	Input (ng)	Imaging QC	Binding Density QC	Positive Control QC	Limit of Detection QC	FOV Count	FOV Counted
1	ABMR-1	5.54	6.3	38.78	0.99	0.17	0.99	6.12	490	485
2	ABMR-2	4.4	3.1	30.8	1	0.2	0.99	9.12	490	490
3	ABMR-3	5.64	4.8	39.48	1	0.19	0.98	7.62	490	480
4	ABMR-4	7.88	N/A	55.16	0.99	0.24	0.98	8.38	490	480
5	ABMR-5	8.62	8.6	60.34	0.99	0.25	0.96	6.75	490	486
6	TCMR-1	7.9	6.8	55.3	1	0.19	0.98	7.12	490	488
7	TCMR-2	6	5.9	42	1	0.16	0.98	7.5	490	488
8	TCMR-3	10.4	5.9	72.8	0.99	0.2	0.99	9.88	490	487
9	TCMR-4	N/A	6.1	N/A	0.99	0.14	0.97	6.64	490	489
10	ATN-1	8.64	8.1	60.48	0.98	0.21	0.98	7	490	484
11	ATN-2	7.08	4.8	49.56	1	0.18	0.98	8.19	490	481
12	ATN-3	5.48	4	38.36	1	0.14	0.98	6.12	490	481

* The nCounter Nanostring platform was conducted for gene profiling using the B-HOT panel. Quality control was done according to the guidelines of Nanostring. Abbreviations: ABMR, antibody-mediated rejection; TCMR, T cell-mediated rejection; ATN, acute tubular necrosis; FOV, Field of View, RIN; N/A, not available; RNA integrity number; QC, quality control.

Proof-of-concept pilot study on the BTM of clinical biopsies to determine clinical potential

Kidney transplant biopsies taken in the context of delayed graft function (DGF) represent a real-world clinical scenario in which fast molecular profiling could reduce the time to tailored treatment. In DGF, the clinical differential diagnosis is often between acute tubular necrosis (ATN), related to the deceased donation procedure, and requiring supportive treatment only, or rejection, which would benefit from timely anti-rejection treatment. Twelve random anonymized BTM samples from clinical renal allograft biopsies with DGF were used for NanoString measurements to investigate whether gene expression profiling can discriminate between these clinical scenarios (Table 4). Principal component analysis (PCA) showed distinct clustering of ATN, antibody-mediated rejection (ABMR), and T cell-mediated rejection (TCMR) (Supplementary Figure 5). A total of 54 genes were differentially expressed (p-value < 0.05 and $|\log2FC| > 1$) between ATN and rejection (ABMR and TCMR together), with 23 genes exhibiting higher expression in the ATN group and 31 genes exhibiting higher expression in the rejection group (Figure 6a). The heatmap of the DGEs further provides preliminary evidence that samples within the rejection group clustered into ABMR and TCMR (Figure 6b). Further DGE analysis between ABMR and TCMR identified 49 genes (p-value < 0.05 and $|\log2FC| > 1$) (Figure 6c), with 12 genes higher in the TCMR group and 37 genes higher in the ABMR group (Figure 6d).

We further investigated the correlation between gene expression in BTM samples and the Banff lesion scores of the corresponding biopsies (Figure 7). Traditional ABMR-related lesions, including peritubular capillaritis (ptc), transplant glomerulopathy (cg), and glomerulitis (g), clustered together and were highly correlated with the genes expressed at higher levels in ABMR. Traditional TCMR-related lesions, including tubulitis (t), interstitial inflammation (i), and total inflammation (ti), clustered together and displayed a strong correlation with the genes expressed at higher levels in TCMR.

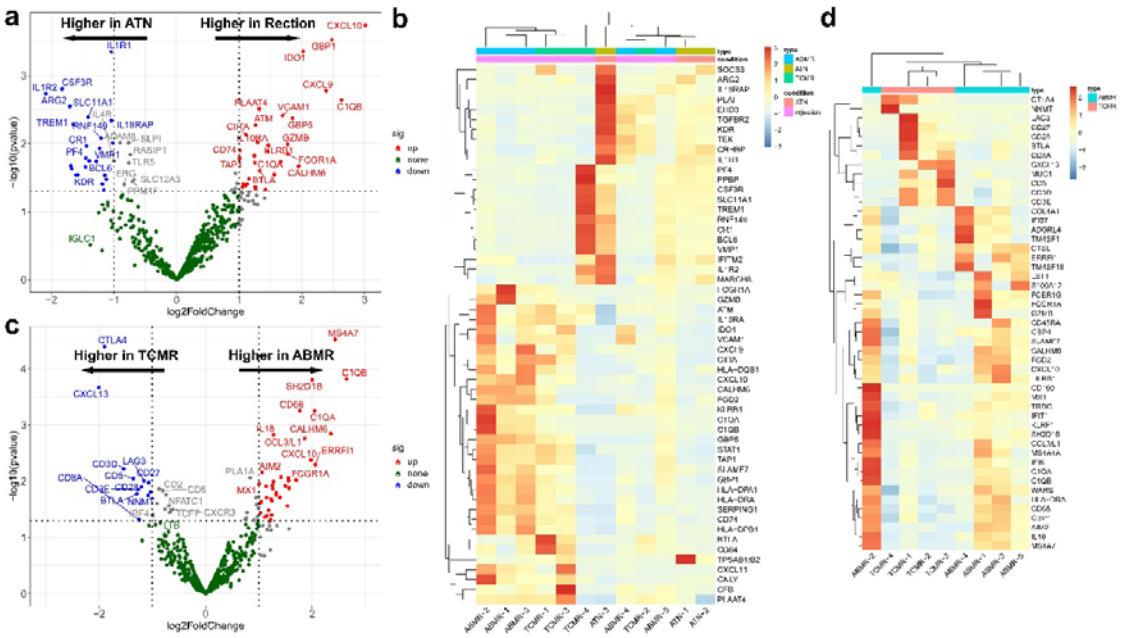

Figure 6. Differentially expressed genes (DEGs) on 12 real BTM. Two volcano plots (a and c) depict B-HOT panel gene expression, with each dot representing a gene. The fold change (FC) is the ratio of mRNA count between two groups. The X-axis represents the log2FC values. The 2 dotted vertical lines on either side of 0 on the X-axis represent |log2FC| = 1. The Y-axis represents the -log10 P value. The horizontal dotted line on the Y-axis represents P-value = 0.05. The blue and red dots are genes that have |log2FC| > 1, respectively, and a P-value < 0.05. Two heatmaps (b and d) show the top DEGs, with each column representing a BTM sample and each row representing a gene. (a) The red dots represent statistically significant genes that are higher in rejection compared to ATN, and the blue dots represent the increased genes in ATN. (b) Hierarchical clustering suggests significant heterogeneity between rejection and ATN. Of the 770 genes, 31 were increased and 23 were reduced in rejection. (c) The red dots represent statistically significant genes that are higher in ABMR compared to TCMR, and the blue dots represent the increased genes in TCMR. (d) Hierarchical clustering suggests significant heterogeneity between ABMR and TCMR. Of the 770 genes, 37 were increased and 12 were reduced in ABMR.

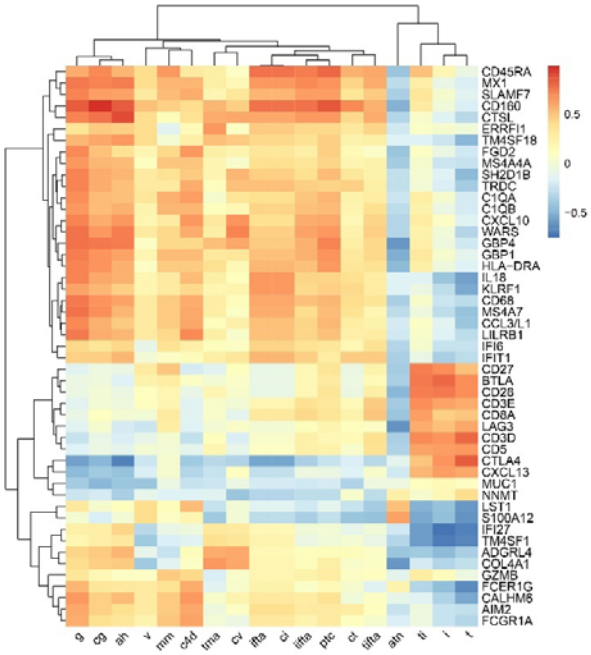

Figure 7. A Spearman's rank correlation heat map comparing the DEGs with Banff lesion scores in real BTM in the setting of delayed graft function. atn, acute tubular necrosis; ti, total interstitial inflammation; i, interstitial inflammation; t, tubulitis; tifta, tubulitis in the area of IFTA; iifta, inflammation in the area of IFTA; ptc, peritubular capillaritis; tma, thrombotic microangiopathy; ct, tubular atrophy; ifta, interstitial fibrosis and tubular atrophy; ci, interstitial fibrosis; v, intimal arteritis; g, glomerulitis; cg, GBM double contours; ah, arteriolar hyalinosis; mm, mesangial matrix expansion; cv, vascular fibrous intimal thickening.

Discussion

In this study, we investigate the technical feasibility of integrating molecular assessment with BTM from biopsies for rapid diagnosis. We optimized and validated the technical methods for RNA isolation and assessed the effect of storage time, determining that samples processed within 24 hours can be assessed without loss of molecular information across the B-HOT transcriptome. Additionally, in a proof-of-concept study, we demonstrated the potential for BTM gene expression profiling to reflect the status of transplanted kidneys, consistent with the Banff lesion score. These findings need further exploration in prospective observational studies.

It is well-recognized that transcriptional profiling reflects global changes in the behavior of a cell[5]. For this reason, and because of the extensive experience with tissue transcriptome analysis in the setting of kidney diseases (mostly transplantation), we focused on transcriptional profiling of the BTM materials. We confirmed the existence of relevant RNA transcripts in BTM fluids and further tested the conditions under which BTM could be processed for RNA analysis. Since RNA easily degrades and expression levels can change over time, the storage time of biopsies stored in BTM is a fundamental factor. Our qPCR data showed that the assessment of BTM samples within 24 hours does not result in loss of molecular information considering the expression of the housekeeping gene HPRT, but also across the targeted transcriptome as measured by the NanoString B-HOT panel (770 genes, ~5% of the full transcriptome). Inside the hospital, the shortest transport time is about half an hour, but these findings suggest that even for consultation cases outside the hospital, the material can be kept stable at 4 □ for at least 24 hours.

To characterize the BTM fluids, we investigated the relationship between BTM and the corresponding frozen tissues in terms of cell distribution via qPCR. We observed a considerably different relative distribution of gene transcripts corresponding to immune and parenchymal cells in BTM. The same phenomenon has been noted via NanoString B-HOT gene panel analysis, indicating the relative enrichment of genes related to immune cells in BTM compared to FFPE. This is expected since parenchymal cells are anchored to each other and to basement membranes and/or collagen fibers through tight and adherents junctions, while immune cells are more easily migrating out of the needle

biopsy. However, this result conveys an advantage for BTM analysis, as phenotyping of inflammatory infiltrates is a hallmark of many kidney diseases. To begin with *CD68*, a marker of macrophages, is in fact highly expressed in BTM. Macrophages were defined as functionally important in different stages of each kidney disease[6]. For instance, their accumulation in the tubulointerstitial area is positively linked to a poor prognosis of lupus nephritis[7]. Additionally in ABMR, intravascular macrophage accumulation in capillaries is described as an indicator of "severe pathologic ABMR"[8]. Also, *CD56* was higher in BTM compared to the corresponding frozen tissues, indicating the potential to capture more Natural killer (NK) cells in the BTM fluids. Based on transcriptomic deconvolution, the estimated fraction of CD56+ NK cells correlated with peritubular capillaritis and glomerulitis [9] and outperformed histological assessment for the prediction of graft failure[10]. Following that, *CD3E*, a T cell marker, and *CD20*, a marker of B cells, were expectedly detectable in the BTM fluids, both of which are involved in various immune-related kidney disorders[11].

The detection of all these biomarkers suggested the potential that BTM might be more appropriate for the diagnosis of (auto) immune-related renal disease and transplant rejection. Our proof-of-concept study confirmed this through B-HOT gene expression profiling on real BTM from transplant biopsies, and certain genes we identified maintain consistency with biomarkers identified from FFPE or biopsy samples[12] as well as histology score.

Upon damage however, parenchymal cells including tubular epithelial cells are also known to be shed into the urine in the form of casts during tubular damage[13] and podocytes can also be found back in the urine in the setting of proteinuric kidney diseases[14]. In line with this, our findings showed that the B-HOT signature correlated specifically with the presence of acute tubular necrosis in the biopsy. In comparison to urine, BTM exhibits additional strength in the presence of endothelial cells, which are likely lacking in urine cytology, because endothelial cells are not lining the luminal space of tubules. Corroborating this, a recent study could annotate 15 cell clusters from urine scRNAseq data, which did not include endothelial cells[15]. It is noteworthy that the endothelial cells marker (*PECAM1*) showed minor differences in expression between BTM and the corresponding frozen. Additionally, genes such as *PLAT* and *GBP1*, which are enriched in endothelial cells, can be detected in BTM fluids

using the NanoString mRNA analysis platform. This indicates that BTM fluids have the potential to identify transplant rejection. Especially in the context of ABMR, which features microvascular inflammation, the importance of endothelial marker detection will need to be investigated[16]. As for the expression of *NPHS1*, a marker of the podocytes, is however markedly lower in the BTM compared to the corresponding frozen tissues. The detachment of podocytes is a characteristic of podocytopathies[17]. Since the nephrectomy samples are not derived from patients with podocytopathies, we cannot confirm the lack of detection of podocytes in BTM fluids of patients with for instance minimal change disease.

The ultimate goal is to achieve a rapid molecular assessment in cases with a limited diagnostic window. Once the biopsy arrives at the pathology department, a liquid biopsy assessment using BTM could be considered as a supplementary pathway before histological assessment. We believe this supplement will be promising and pivotal to assist clinical physicians with urgent therapeutic intervention. Particularly for the rapidly progressive renal disease, such as the transplanted kidney susceptible to acute rejection, which has been identified as a significant factor in diminished allograft survival in earlier research[18], and was reconsidered as a potential indicator leading to prolonged graft dysfunction[19]. Timely and targeted treatment will thereby start graft attrition at a higher intercept and lead to better long-term outcomes[20]. BTM, as a new resource that carries biological information related to the corresponding biopsy, has a noticeable advantage in being easily accessible, as it only is a waste product during the sample transport process. This contrasts with other molecular diagnostic technologies, which often require additional or processed tissues. In addition, BTM can be applied to quickly detect specific RNA transcripts associated with kidney conditions, which is more objective and less experience required compared to microscope assessment. The transcriptomic information obtained from BTM is encouraging. It would be promising to achieve the same-day diagnosis integrating BTM with qPCR technology could enable same-day diagnosis, as the entire procedure could be completed within 8 hours if everything is well-organized.

In conclusion, our results demonstrate that RNA obtained from BTM is of sufficient quality for gene expression analysis. BTM represents a promising new liquid biopsy material for rapid molecular

assessment in cases with narrow diagnostic windows (e.g., severe glomerulonephritis or vasculitis, transplant rejection). In fact, this method is not limited to kidney biopsies; it can be optimized for any fresh sample being transported to the pathology department. Future research will focus on developing targeted gene panels for primary discrimination between clinically relevant differential diagnoses to guide initial treatment choices and prevent further organ damage in case of aggressive disease presentations.

Disclosure

The authors declare there are no conflicts of interest.

Acknowledgments

The study was supported by the China Scholarship Council (CSC). We would like to acknowledge Ron Wolterbeek (Department of Biomedical Data Sciences, Medical Statistics, Leiden University Medical Centre, Leiden, The Netherlands) for support.

Reference

1. Randhawa P. The MMDx((R)) diagnostic system: A critical re-appraisal of its knowledge gaps and a call for rigorous validation studies. *Clin Transplant* 2022; **36:** e14747.
2. Mengel M, Loupy A, Haas M, *et al.* Banff 2019 Meeting Report: Molecular diagnostics in solid organ transplantation-Consensus for the Banff Human Organ Transplant (B-HOT) gene panel and open source multicenter validation. *Am J Transplant* 2020; **20:** 2305-2317.
3. Nanostring-Technologies: Gene_list_LBL-10743-01_Human_Organ_Transplant_Panel. In, 2019
4. Alam O. A single-cell-type transcriptomics map of human tissues. *Nat Genet* 2021; **53:** 1275-1275.
5. Wang Z, Gerstein M, Snyder M. RNA-Seq: a revolutionary tool for transcriptomics. *Nat Rev Genet* 2009; **10:** 57-63.
6. Anders HJ, Ryu M. Renal microenvironments and macrophage phenotypes determine progression or resolution of renal inflammation and fibrosis. *Kidney Int* 2011; **80:** 915-925.

7. Chen J, Cui L, Ouyang J, *et al.* Clinicopathological significance of tubulointerstitial CD68 macrophages in proliferative lupus nephritis. *Clin Rheumatol* 2022; **41:** 2729-2736.

8. Glass C, Butt YM, Gokaslan ST, *et al.* CD68/CD31 immunohistochemistry double stain demonstrates increased accuracy in diagnosing pathologic antibody-mediated rejection in cardiac transplant patients. *Am J Transplant* 2019; **19:** 3149-3154.

9. Dos Santos DC, Saraiva Camara NO, David DSR, *et al.* Expression patterns of CD56+ and CD16+ cells in renal transplant biopsies with acute rejection: Associations with microcirculation injuries and graft survival. *Nephrology (Carlton)* 2017; **22:** 993-1001.

10. Yazdani S, Callemeyn J, Gazut S, *et al.* Natural killer cell infiltration is discriminative for antibody-mediated rejection and predicts outcome after kidney transplantation. *Kidney International* 2019; **95:** 188-198.

11. Yatim KM, Lakkis FG. A Brief Journey through the Immune System. *Clin J Am Soc Nephro* 2015; **10:** 1274-1281.

12. Haas M, Loupy A, Lefaucheur C, *et al.* The Banff 2017 Kidney Meeting Report: Revised diagnostic criteria for chronic active T cell-mediated rejection, antibody-mediated rejection, and prospects for integrative endpoints for next-generation clinical trials. *American Journal of Transplantation* 2018; **18:** 293-307.

13. Cavanaugh C, Perazella MA. Urine Sediment Examination in the Diagnosis and Management of Kidney Disease: Core Curriculum 2019. *Am J Kidney Dis* 2019; **73:** 258-272.

14. Iampietro C, Bellucci L, Arcolino FO, *et al.* Molecular and functional characterization of urine-derived podocytes from patients with Alport syndrome. *J Pathol* 2020; **252:** 88-100.

15. Latt KZ, Heymann J, Jessee JH, *et al.* Urine Single-Cell RNA Sequencing in Focal Segmental Glomerulosclerosis Reveals Inflammatory Signatures. *Kidney Int Rep* 2022; **7:** 289-304.

16. de Kort H, Willicombe M, Brookes P, *et al.* Microcirculation inflammation associates with outcome in renal transplant patients with de novo donor-specific antibodies. *Am J Transplant* 2013; **13:** 485-492.

17. Kopp JB, Anders HJ, Susztak K, *et al.* Podocytopathies. *Nat Rev Dis Primers* 2020; **6:** 68.

18. Almond PS, Matas A, Gillingham K, *et al.* Risk factors for chronic rejection in renal allograft recipients. *Transplantation* 1993; **55:** 752-756; discussion 756-757.

19. El Ters M, Grande JP, Keddis MT, *et al.* Kidney allograft survival after acute rejection, the value of follow-up biopsies. *Am J Transplant* 2013; **13:** 2334-2341.

20. Lamb KE, Lodhi S, Meier-Kriesche HU. Long-term renal allograft survival in the United States: a critical reappraisal. *Am J Transplant* 2011; **11:** 450-462.

Supplemental Figures

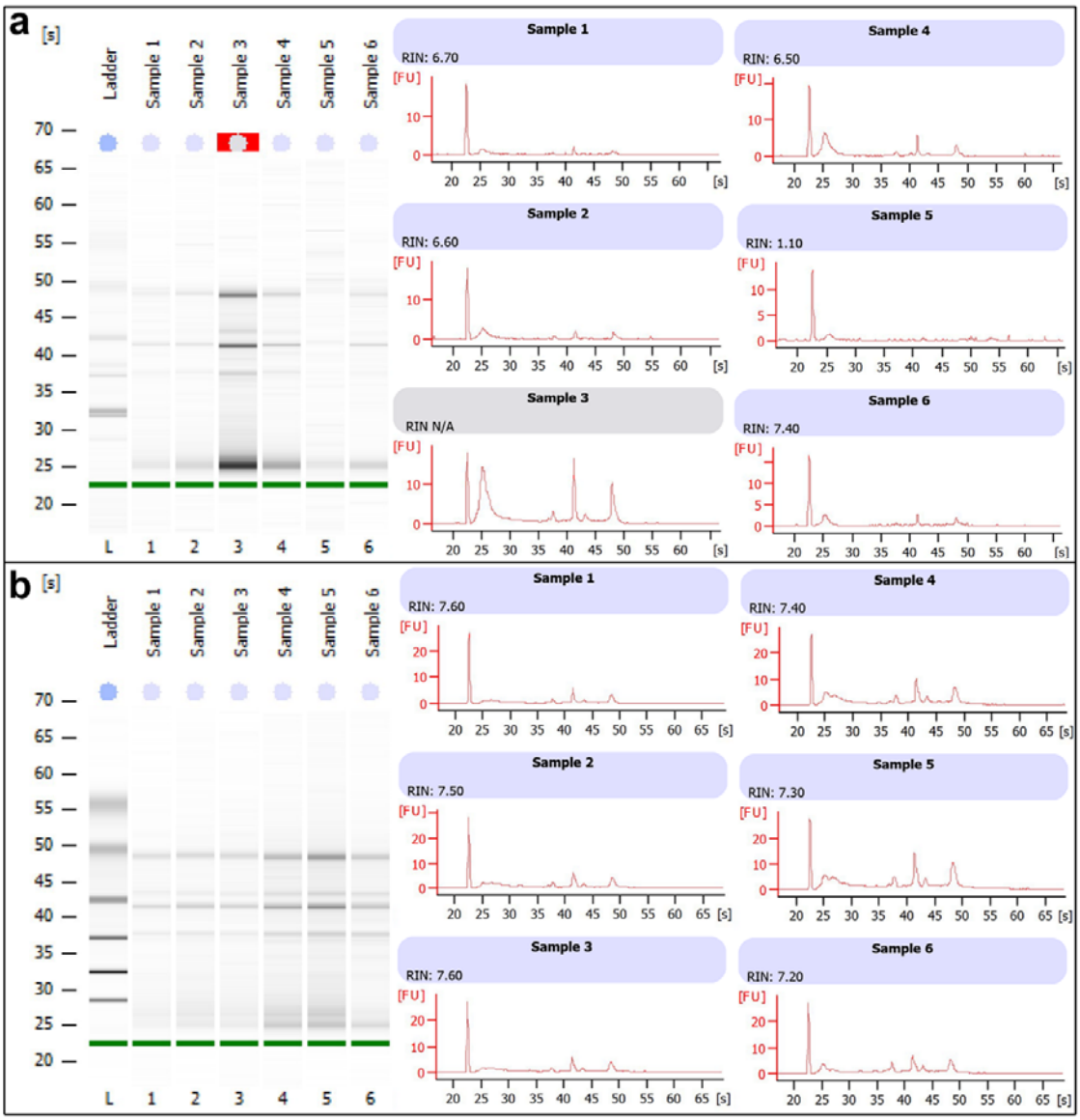

Supplementary Figure 1. The RNA integrity assay: TRIzol method vs TRIzol method plus RNeasy clean-up. The high-intensity band and highest peak between 40 and 45 represent 18S ribosomal RNA, while the peak between 45 and 50 represents 28S ribosomal RNA. (a) The RNA was isolated from 6 samples using only the TRIzol method. Sample 3 shows an "N/A" warning, indicating that the RIN may be unreliable. Sample 5 does not show a high-intensity band in the gel image and has an extremely low RIN value of 1.1. (b) The RNA was isolated from another 6 samples, which were derived from the same kidney, using the TRIzol method plus the RNeasy Kit. This method shows higher RIN values with less variation after the RNeasy clean-up procedure compared to TRIzol alone.

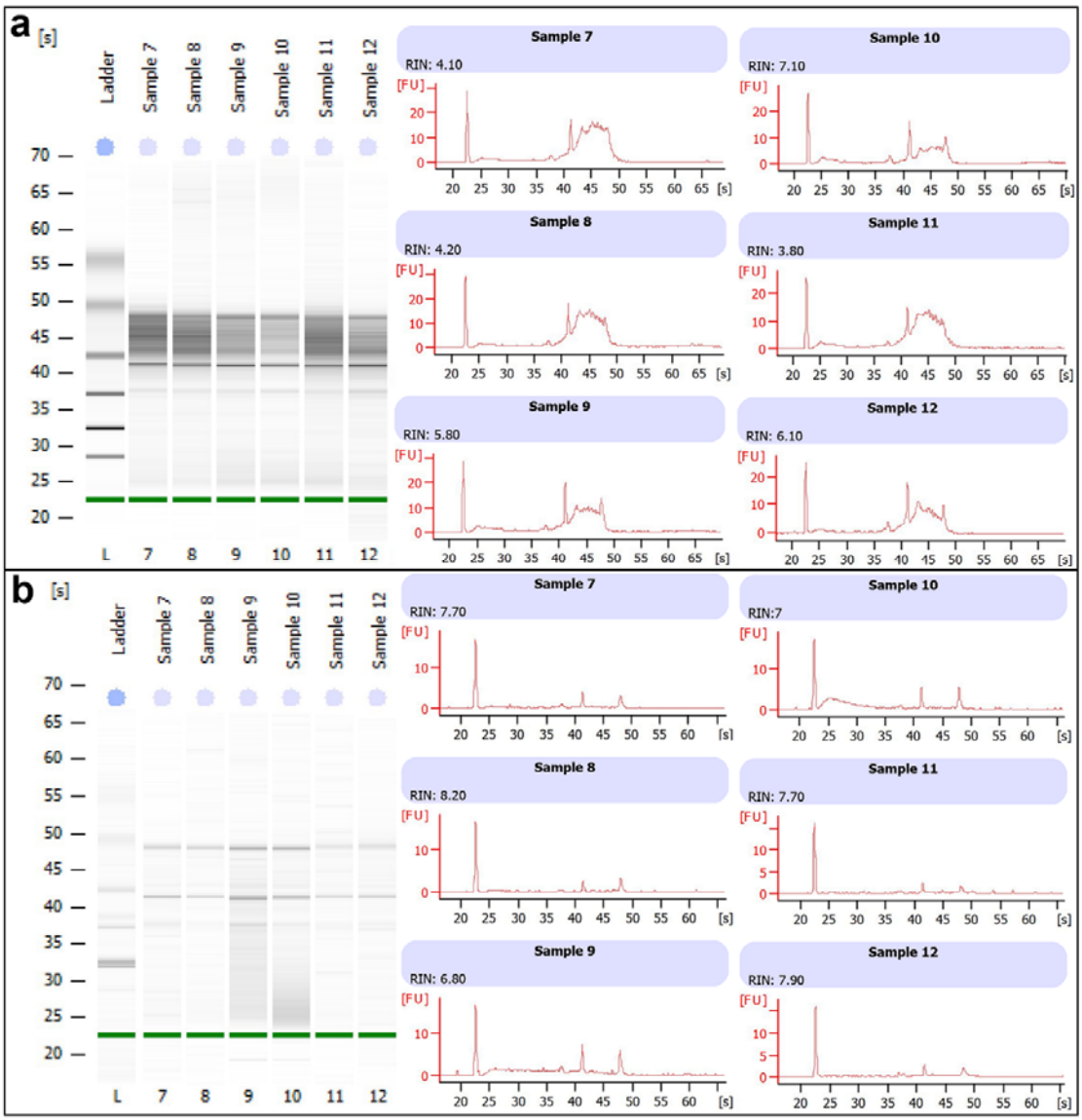

Supplementary Figure 2. The RNA integrity assay: RNeasy with and without DNase treatment. The high-intensity band and highest peak between 40 and 45 represent 18S ribosomal RNA, while the peak between 45 and 50 represents 28S ribosomal RNA. (a) The RNA was isolated from all samples using RNeasy without DNase treatment. The presence of dark backgrounds and broad peaks between 18S and 28S suggests contamination with genomic DNA. (b) RNA was isolated from another 6 samples, derived from the same kidney, using RNeasy with DNase treatment. This method shows clear bands in the gel image and higher RIN values after DNase treatment compared to the previous results.

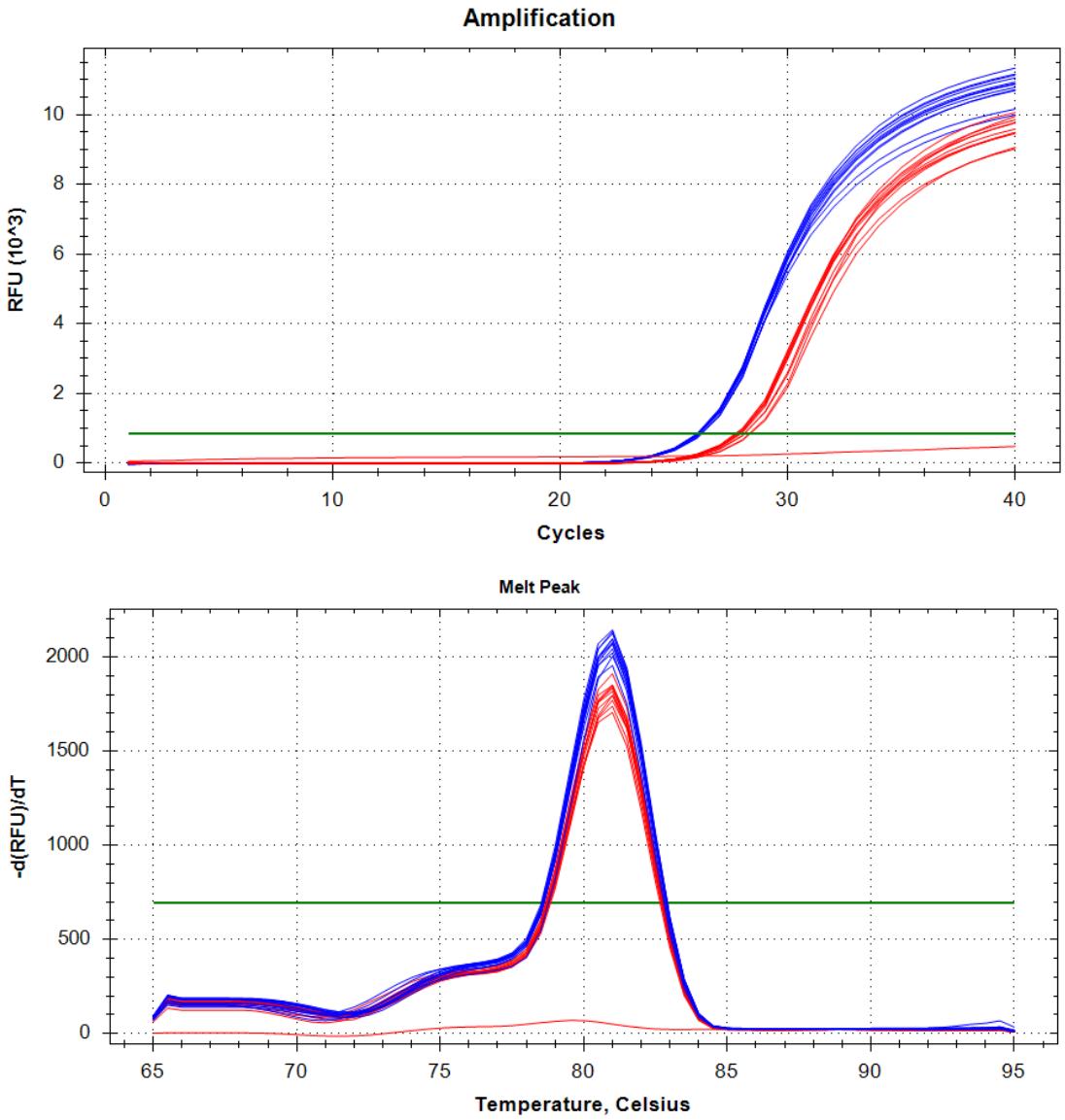

Supplementary Figure 3 Repeated qPCR measurements on two groups of identical samples to show the inter-assay coefficient of variance (ICV). Different colors represent different groups. Each group consists of twelve identical samples. The results show a high degree of consistency within each group, regardless of amplification or melt peak.

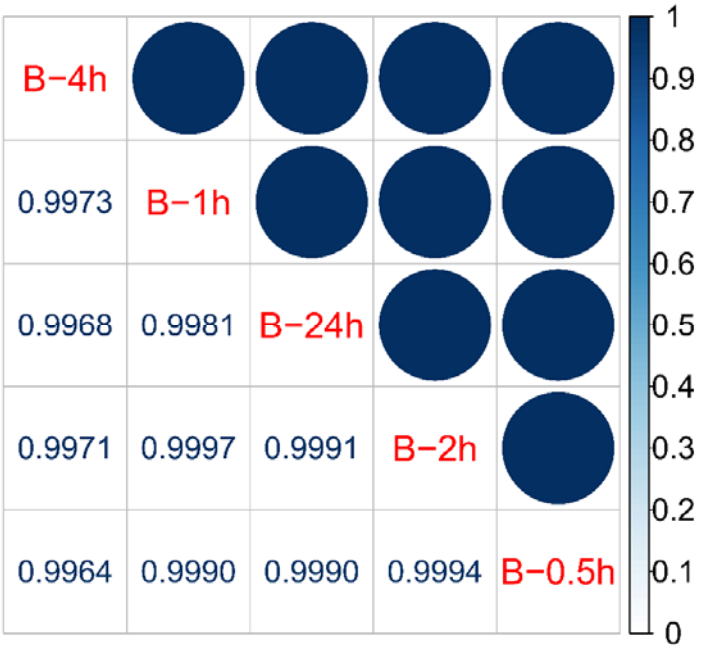

Supplementary Figure 4. Correlation matrix for NanoString B-HOT expression among BTM storage times. A strong correlation between the gene expression of the B-HOT panel among the five storage time points (all R >0.99).

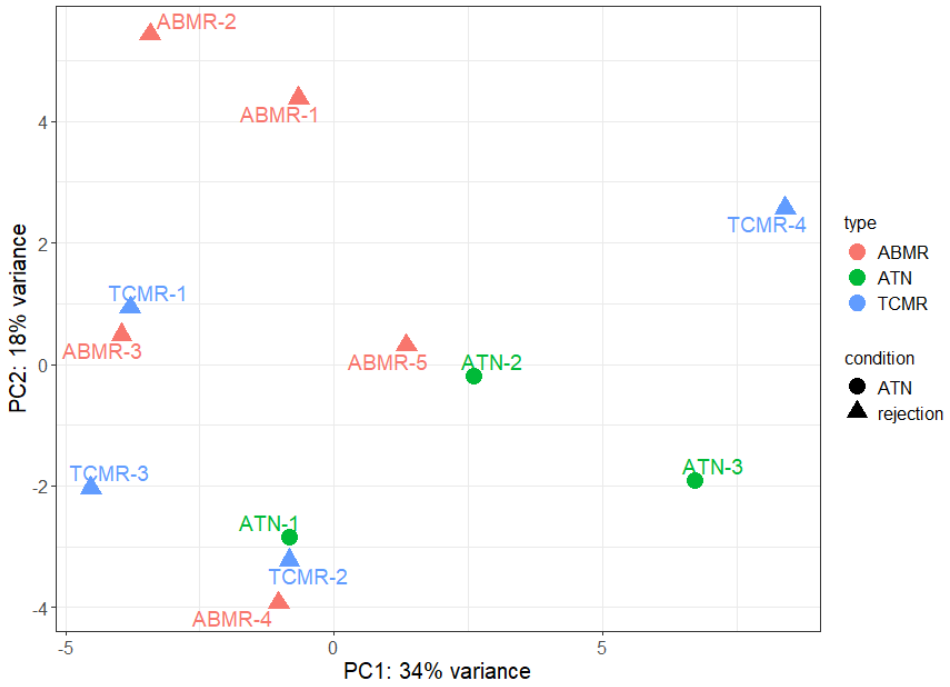

Supplementary Figure 5. Principal component analysis (PCA) plot of the ATN and rejection (ABMR and TCMR) samples using 770-gene B-HOT panel. The expression level was normalized using the "rlog" function in "DESeq2," which transformed the data to the log2 scale.